








RESEARCH ARTICLE
10.1029/2022MS003040

Assimilation of Remotely Sensed Leaf Area Index Enhances the Estimation of Anthropogenic Irrigation Water Use

Wanshu Nie¹ , Sujay V. Kumar² , Christa D. Peters-Lidard³ , Benjamin F. Zaitchik¹ ,
Kristi R. Arsenault^{2,4} , Rajat Bindlish², and Pang-Wei Liu^{2,5}

¹Department of Earth and Planetary Sciences, Johns Hopkins University, Baltimore, MD, USA, ²Hydrological Science Laboratory, NASA Goddard Space Flight Center, Greenbelt, MD, USA, ³Earth Science Division, NASA Goddard Space Flight Center, Greenbelt, MD, USA, ⁴Science Applications International Corporation, McLean, VA, USA, ⁵Science Systems and Applications Inc., Lanham, MD, USA

Key Points:

- Moderate Resolution Imaging Spectroradiometer leaf area index (LAI) data are assimilated into the Noah-MP land surface model to inform simulation of irrigation schedules and volumes
- Irrigation simulations without LAI assimilation overestimate irrigation amount and increase the BIAS for evapotranspiration (ET) and GPP
- Assimilating LAI to constrain irrigation shows the overall best performance for surface soil moisture, ET, and GPP

Correspondence to:

W. Nie,
nwanshu1@jhu.edu

Citation:

Nie, W., Kumar, S. V., Peters-Lidard, C. D., Zaitchik, B. F., Arsenault, K. R., Bindlish, R., & Liu, P.-W. (2022). Assimilation of remotely sensed leaf area index enhances the estimation of anthropogenic irrigation water use. *Journal of Advances in Modeling Earth Systems*, 14, e2022MS003040. <https://doi.org/10.1029/2022MS003040>

Received 9 FEB 2022
Accepted 11 OCT 2022

Abstract Representation of irrigation in Earth System Models has advanced over the past decade, yet large uncertainties persist in the effective simulation of irrigation practices, particularly over locations where the on-ground practices and climate impacts are less reliably known. Here we investigate the utility of assimilating remotely sensed vegetation data for improving irrigation water use and associated fluxes within a land surface model. We show that assimilating optical sensor-based leaf area index estimates significantly improves the simulation of irrigation water use when compared to the USGS ground reports. For heavily irrigated areas, assimilation improves the evaporative fluxes and gross primary production (GPP) simulations, with the median correlation increasing by 0.1–1.1 and 0.3–0.6, respectively, as compared to the reference datasets. Further, bias improvements in the range of 14–35 mm mo⁻¹ and 10–82 g m⁻² mo⁻¹ are obtained in evaporative fluxes and GPP as a result of incorporating vegetation constraints, respectively. These results demonstrate that the use of remotely sensed vegetation data is an effective, observation-informed, globally applicable approach for simulating irrigation and characterizing its impacts on water and carbon states.

Plain Language Summary Agricultural irrigation accounts for more than 70% of freshwater use over the globe and can impact local and regional water resources, crop productivities, and climate and weather systems. Investigating impact of irrigation heavily relies on models, which vary in terms of modeling structure, input data sources, assumptions, etc. Given these variations, models are often subject to large uncertainties in estimating irrigation water use. The goal of this study is to explore the potential to integrate satellite observations of vegetation conditions with models to improve estimates of irrigation and its impact across the Contiguous United States. We find that integrating satellite observations is helpful in correcting simulation of vegetation growth, leading to a better estimation of irrigation water use and its impact on surface soil moisture, evapotranspiration, and agricultural productivities. These results underscore the effectiveness of using satellite vegetation observations to improve irrigation modeling.

1. Introduction

Globally, irrigation is the largest water use sector, accounting for 70% of freshwater withdrawals (Frenken & Gillet, 2012). The role it plays in modifying surface and groundwater systems (Asoka et al., 2017; Kustu et al., 2011; Leng et al., 2015; Rodell et al., 2018; Scanlon et al., 2012), agricultural productivity (Troy et al., 2015; Zaveri & Lobell, 2019), and land-atmosphere interactions (DeAngelis et al., 2010; Kueppers et al., 2007; Kustu et al., 2011; Lawston et al., 2020; Lobell et al., 2008; Zeng et al., 2017) is well established in intensively irrigated regions across the globe at various spatiotemporal scales. In recognition of the importance of representing the human water footprint for a better description of hydrological and biogeochemical processes, a large number of modeling studies (Döll et al., 2012; Leng et al., 2014; Nie et al., 2018; Pokhrel et al., 2015; Wada et al., 2014) have incorporated irrigation schemes in Earth System Models (ESMs). Despite these advances, uncertainties in capturing the subjective on-ground practices, climate and agricultural datasets, or modeling parameterizations remain a challenge in capturing the timing, magnitude, and spatial patterns of irrigation water use (Scanlon et al., 2018; Wisser et al., 2008; Wada et al., 2017).

Irrigation demand, and the associated surface and groundwater extractions, are highly correlated to climate variability and crop phenology (Deines et al., 2017; Nie et al., 2021; Russo & Lall, 2017). Estimating irrigation

© 2022 The Authors. Journal of Advances in Modeling Earth Systems published by Wiley Periodicals LLC on behalf of American Geophysical Union. This is an open access article under the terms of the [Creative Commons Attribution-NonCommercial License](https://creativecommons.org/licenses/by/4.0/), which permits use, distribution and reproduction in any medium, provided the original work is properly cited and is not used for commercial purposes.

demand in response to climate variability is of high importance especially during times of water resource stress such as droughts. However, this is often challenging as irrigation applications may vary due to water shortages or restrictions while the use of conceptualized irrigation rules within ESMs is limited in representing such cases. Modeling efforts have been undertaken to improve the representation of human water use in ESMs, but relatively few have focused on characterizing sub-annual and interannual variations of irrigation water use. Specific limitations in the irrigation parameterizations include: (a) ignoring the sources of irrigation withdrawals (Lawston et al., 2015; Yilmaz et al., 2014); (b) using static irrigation land use or source water partitions obtained from datasets for a specific year (Leng et al., 2014; Pokhrel et al., 2015); (c) irrigating based on a climatologically fixed growing season that does not account for management responses to extremes such as drought (Leng et al., 2014; Lawston et al., 2015; Yilmaz et al., 2014); and (d) calibrating models using nonphysical parameters that may not provide skill in future water use projections (Döll et al., 2012). A few studies that employed the active simulation of vegetation phenology were able to better represent interannual changes in irrigation (Flörke et al., 2010; Wu et al., 2018; Zhao et al., 2015). However, significant uncertainties remain in many ESMs in predicting the vegetation response to changes in hydroclimate (Ma et al., 2017; Niu et al., 2020; Trugman et al., 2018). Further, the reported improvements in the irrigation formulations are either limited to certain vegetation types and crop species (Liu et al., 2016) or rely heavily on field level calibration (Li et al., 2021).

Recognizing these limitations, several efforts have incorporated observational constraints of vegetation states such as Leaf Area Index (LAI) and vegetation optical depth (VOD) within models through data assimilation, aiming to improve the estimates of terrestrial carbon fluxes via combined process-based and data-driven models (Demarty et al., 2007; Kumar et al., 2019, 2020; Mocko et al., 2021). These studies have demonstrated improved representation of not only vegetation conditions and the associated carbon fluxes, but also soil moisture, stream-flow, and evapotranspiration (ET), as well as the representation of extreme events (Albergel et al., 2017; Barbu et al., 2014; Ines et al., 2013; Kumar et al., 2019; Mocko et al., 2021; Xie et al., 2017). Though crop phenology is one of the key factors reflecting the irrigation needs, so far, no studies have quantitatively analyzed the impact of assimilating LAI on long-term irrigation estimation, which is the main objective for this study.

In a previous study (Nie et al., 2021), an optimal set of irrigation simulations across the Contiguous United States (CONUS) was developed by incorporating time-varying irrigation fraction and source water partitioning datasets at 5-year intervals into the Noah-MP land surface model. Building upon that, here we investigate whether assimilating the remote sensing-based LAI product can improve irrigation estimation and the associated water, energy, and carbon fluxes for several major irrigated water resource regions. While Nie et al. (2021) established a reasonably well-estimated spatiotemporal distribution of irrigation water use, the approach relied on a climatological, monthly time-varying green vegetation fraction (GVF) data set, which prescribed vegetation states instead of prognostically simulating vegetation growth. That is, the Nie et al. (2021) approach is restricted to the deterministic, diagnostic simulation of irrigation impacts on vegetation states, as opposed to approaches integrated with an active vegetation model with forecast and projection capabilities. The use of the climatological vegetation data also restricts the ability to simulate the interannual changes in irrigation water use influenced by corresponding vegetation changes.

In this study, our primary goal is to evaluate the benefit of assimilating remote sensing-based LAI to improve the prognostically represented irrigated vegetation phenology and the interactive impact of vegetation phenology and irrigation on associated fluxes. To isolate these impacts, we perform simulations with and without assimilating LAI and simulations with and without irrigation actively represented. Irrigation estimates from USGS water use reports and satellite-derived estimates of surface soil moisture, ET, and gross primary production (GPP) are used to evaluate the simulations. Quantifying the influence of assimilating vegetation states in improving irrigation is important because an effective correction in vegetation conditions and the associated irrigation scheduling has the potential to reduce the dependency and sensitivity of irrigation formulations on empirical and simplistic parameterizations. The use of vegetation remote sensing information provides a generalized, globally applicable approach to prescribe irrigation onset and water use estimation within models.

2. Methods

2.1. Model Configuration

All simulations are conducted using the Noah-MP LSM (Niu et al., 2011), Version 4.0.1, implemented within the framework of the NASA Land Information System (LIS; Kumar et al., 2006) (open source software available

at <https://github.com/NASA-LIS/LISF>). Noah-MP is applied in offline mode (not coupled to an atmospheric model) at 0.125° spatial resolution over the CONUS region for period 2003–2019 after a 55-year spin-up, and is driven by the meteorological inputs from North America Land Data Assimilation System Phase 2 (NLDAS2; Xia et al., 2012). The model is configured using the Moderate Resolution Imaging Spectroradiometer–International Geosphere Biosphere Program (MODIS-IGBP; Friedl et al., 2010) land cover data set at 1 km, the machine learning based 250-m soil property and class data set generated at the International Soil Reference Information Centre (ISRIC; Hengl et al., 2017), and the Multi-Error-Removed Improved-Terrain (MERIT; Yamazaki et al., 2017) elevation at 3-arcsec spatial resolution. MERIT elevation map is developed to eliminate major error components such as stripe noise and speckle noise based on the NASA Shuttle Radar Topography Mission (Farr et al., 2007). In this study, the prognostic vegetation module (Dickinson et al., 1998) is enabled, along with a Ball-Berry photosynthesis-based stomatal resistance scheme (Ball et al., 1987; Bonan, 1996; Collatz et al., 1991), to simulate the carbon uptake and allocation among leaf, stem, wood, and root. LAI is calculated from leaf carbon mass by multiplying by the specific leaf area, which is a vegetation type dependent parameter. The greenness vegetation fraction (GVF), which divides a grid cell into a fractional vegetated area and a fractional bare ground area, is derived from LAI based on the following function:

$$\text{GVF} = 1 - e^{-0.52\text{LAI}} \quad (1)$$

GVF is an important variable in Noah-MP, which plays an essential role in representing vegetation conditions, partitioning evapotranspiration into different components, and determining the timing and amount for irrigation. Rather than prescribing GVF as a vegetation parameter, which is widely applied in other land surface modeling applications, here GVF is updated based on LAI within the prognostic vegetation module. This is critical for places with intensely irrigated agriculture as the interaction among the prognostic vegetation module, the irrigation scheme, and data assimilation enables the model to simulate the interannual variability of irrigation water use. This in turn, can influence the subsequent vegetation growth and soil moisture conditions.

2.2. Irrigation in Noah-MP

The irrigation scheme was originally built into Noah-MP based on a soil moisture deficit approach (Ozdogan et al., 2010) and further adapted by Nie et al. (2018, 2021) to account for the spatiotemporal variability of irrigation area and source water partitioning. For simulations with irrigation, the irrigation water use is estimated based on four rules: (a) where to irrigate; (b) when to irrigate; (c) how much water to irrigate; and (d) what are the irrigation sources (i.e., surface water vs. groundwater irrigation).

The MODIS Irrigated Agriculture Data set for the United States (MIrAD-US; Brown & Pervez, 2014), updated every 5 years, is used to provide the percentage of irrigated area within each model grid cell. It is used in combination with the MODIS-IGBP land cover map to restrict the irrigatable area within certain land cover types such as croplands and grasslands.

The timing of irrigation is determined by using a vegetation threshold parameter (GVF_{TS}). Whenever the GVF value exceeds GVF_{TS} , the period is defined as the effective growing season during which irrigation can occur if other criteria are satisfied. GVF_{TS} is calculated as:

$$\text{GVF}_{\text{TS}} = \text{GVF}_{\text{min}} + (A + B \cdot (\text{GVF}_{\text{max}} - \text{GVF}_{\text{min}})) \cdot (\text{GVF}_{\text{max}} - \text{GVF}_{\text{min}}) \quad (2)$$

in which GVF_{max} and GVF_{min} are the maximum and minimum GVF with respect to long-term climatology (2003–2019 in this study), representing the long-term range of the vegetation greenness for each grid cell. A and B are user-identified vegetation parameters used to control the range of GVF for which irrigation is triggered.

During the effective growing season, the model checks the plant accessible root zone soil water amount ($\text{SWS}_{\text{avail}}$) at 6 a.m. local time every day and if $\text{SWS}_{\text{avail}}$ is dryer than a soil moisture deficit threshold, C , irrigation will be triggered. $\text{SWS}_{\text{avail}}$ is estimated as:

$$\text{SWS}_{\text{avail}} = \frac{\sum_{i=1}^{l_{\text{root}}} \theta_i * \text{RD}_i - \sum_{i=1}^{l_{\text{root}}} \theta_w * \text{RD}_i}{\sum_{i=1}^{l_{\text{root}}} \theta_c * \text{RD}_i - \sum_{i=1}^{l_{\text{root}}} \theta_w * \text{RD}_i} \quad (3)$$

in which θ_i and RD_i are the soil moisture content and rooting depth at the i th soil layer respectively, θ_w is the wilting point and θ_c is the field capacity for the corresponding soil type in the grid cell. l_{root} is the number of soil layers that the rooting depth has reached, where the rooting depth is estimated as:

$$RD = GVF \cdot RD_{max} \quad (4)$$

RD_{max} is the maximum rooting depth as a function of the crop type, and in our simulation, it is set to 1.2 m in the representation of the generic row crops. Note that vegetation related parameters A , B and soil moisture related parameter C are all determined in a benchmark simulation described in Section 2.4.

Once irrigation is triggered, the irrigation amount required to bring the current root zone soil moisture condition up to field capacity is calculated. The irrigation rate (Q_{irrig}) is then estimated by distributing the amount evenly during the irrigation occurring period (t_{irrig}), which is set to be local time 6–10 a.m.:

$$Q_{irrig} = \frac{\sum_{i=1}^{l_{root}} (\theta_c - \theta_i) * RD_i}{t_{irrig}} \quad (5)$$

To allocate surface water and groundwater sources to irrigation demand, the USGS-based groundwater irrigation percentage datasets (<https://water.usgs.gov/watuse/data/>), updated every 5 years, are used to generate the groundwater irrigation ratio (GW_{ratio}) for each grid cell, and the groundwater storage (WA) at time t is then updated by:

$$WA_t = WA_{t-1} - Q_{irrig} * GW_{ratio} * \Delta t \quad (6)$$

in which Δt is the model time step, which is set to be 15 min.

2.3. LAI Data Assimilation

The one-dimensional Ensemble Kalman Filter (EnKF; Reichle et al., 2002) is used to assimilate LAI into Noah-MP. The assimilation update is determined by the relative uncertainty between the LAI observations and the model ensemble:

$$X_{T+}^i = X_{T-}^i + K_T (Z_T^i - H_T X_{T-}^i) \quad (7)$$

in which X_{T-}^i and X_{T+}^i are the i th ensemble member of the state vectors before and after the assimilation update, respectively. Z_T^i is the observation vector that is assimilated into the model. H_T is an operator that converts the model states to observation space. The Kalman gain matrix K_T determines the relative weights of uncertainties in the model and LAI observations.

The uncertainty of the model is estimated from an ensemble of model simulations, developed by applying small perturbations to three meteorological fields (i.e., precipitation (P), incident shortwave (SW) and longwave (LW) radiation) and LAI state variable following Kumar et al. (2019). Time series correlations are imposed via a first-order regressive model (AR(1)) with a timescale of 1 day for both forcing fields and LAI state. Cross correlations of the perturbations are set within the forcing fields based on known associations between these components (Reichle et al., 2007). For instance, a positive perturbation to SW tends to be associated with negative perturbations to LW and P. Additive perturbation with a standard deviation of 0.01 (–) is applied for both modeled and observed LAI fields. A summary of the perturbation settings is listed in Table 1. Note that after LAI gets updated by data assimilation, the leaf biomass is updated by dividing the LAI with the specific leaf area, and the GVF is also updated based on Equation 1.

2.4. Experimental Design

In this study, the two vegetation parameters (A and B) and one soil moisture parameter (C) for the domain are defined based on Nie et al. (2021), in which the simulated irrigation water use was evaluated against the USGS water use report for 2005, 2010, and 2015 at state level. Besides, annual irrigation water use for 2002–2017 and its response to climate variability were evaluated for the four most intensively irrigated states (i.e., California, Texas, Kansas, and Mississippi) where year-by-year irrigation water reports are available. In this configuration,

Table 1
Ensemble Perturbation Parameters in the Assimilation Simulations

Variable	Type	Standard deviation	Temporal correlation	Perturbation cross-correlations		
Met-forcings				SW	LW	P
SW	M	0.2 (dimensionless)	1 day	1	-0.5	-0.8
LW	A	30 W m ⁻²	1 day	-0.5	1	0.5
P	M	0.5 (dimensionless)	1 day	-0.8	0.5	1
LSM States						
LAI	A	0.01 m ² m ⁻²	1 day			

Note. Multiplicative (M) or Additive (A) perturbations are applied to incident shortwave radiation (SW), incident longwave radiation (LW), precipitation (P), and leaf area index (LAI).

the prognostic phenology module is turned off, and the climatological monthly time-varying GVF data sets derived from MODIS-NDVI are used to inform the timing of the growing season to trigger irrigation. This set of irrigation parameters is then used in the following two sets of experiments with the prognostic phenology scheme turned on:

Open Loop Experiments (OL and OL_{irr}): The model is run without assimilating any vegetation observations. Both experiments are run with prognostic phenology module, but with irrigation turned off for OL and on for OL_{irr}.

MODIS-Based LAI Assimilation (DA and DA_{irr}): In the DA and DA_{irr} experiments, the gap-filled and interpolated daily LAI retrievals obtained from the MODIS-MCD15A2H Version 6 product (Myneni et al., 2015) are assimilated into Noah-MP. An ensemble size of 20 is generated by applying perturbations to three meteorological fields (i.e., precipitation, incident shortwave, and longwave radiation) and LAI state variable following Kumar et al. (2019). Irrigation is turned off for DA and on for DA_{irr}.

We first compare the simulated and USGS reported irrigation water amount at the state level to see the influence of LAI assimilation on irrigation estimation. USGS-based irrigation estimates for 2005, 2010, and 2015 are used as the reference datasets for evaluation. We then compare the two sets of simulations to investigate the isolated and combined impact of irrigation and LAI assimilation on the water, energy, and carbon fluxes for irrigation managed regions. Datasets utilized for this evaluation include: (a) the 1 km gridded soil moisture data derived from the Soil Moisture Active Passive (SMAP) Level 2 Enhanced soil moisture product (Chan et al., 2018) covering the period of 2015–2019 using the Thermal Hydraulic disaggregation of Soil Moisture (THySM) (Chen et al., 2022; Liu et al., 2022) approach; (b) the gridded 5 km daily Atmosphere-Land Exchange Inverse (ALEXI; Anderson et al., 2007) evapotranspiration for the period of 2003–2019; and (c) the gridded 5 km daily estimates of GPP from FluxSat (Joiner et al., 2018) for the period of 2003–2019. It should be noted that the FluxSat GPP product uses MODIS reflectance information along with remote sensing-based solar induced fluorescence calibrated to ground measurements. Similarly, the THySM product is derived based on combining thermal inertia theory and soil infiltration process that utilizes the land surface temperature and NDVI from MODIS and soil texture from ISRIC to enhance SMAP's original spatial resolution. The version of ALEXI ET data used here relies on time differential land surface temperature from geostationary satellites. Although these reference datasets may contain some common information to that of MODIS LAI datasets assimilated in this study, they also incorporate other unique information as indicated above, which is independent from LAI.

3. Results

3.1. Irrigation Water Amount

For this study, we select nine water resource regions for analyses, covering the most intensively irrigated area with wide variety in source water partitioning (Figure 1). The Lower Mississippi Region (LMR), the High Plains across the Missouri Region (MR), the Arkansas-White-Red Region (AWRR), and the Texas Gulf region (TGR) include intensively irrigated areas primarily supported by groundwater pumping for irrigation. The western regions including the Central Valley in California Region (CR), the Pacific Northwest Region (PNR) along the Snake River, and the eastern regions with smaller irrigation extent including the Great Lakes Region (GLR),

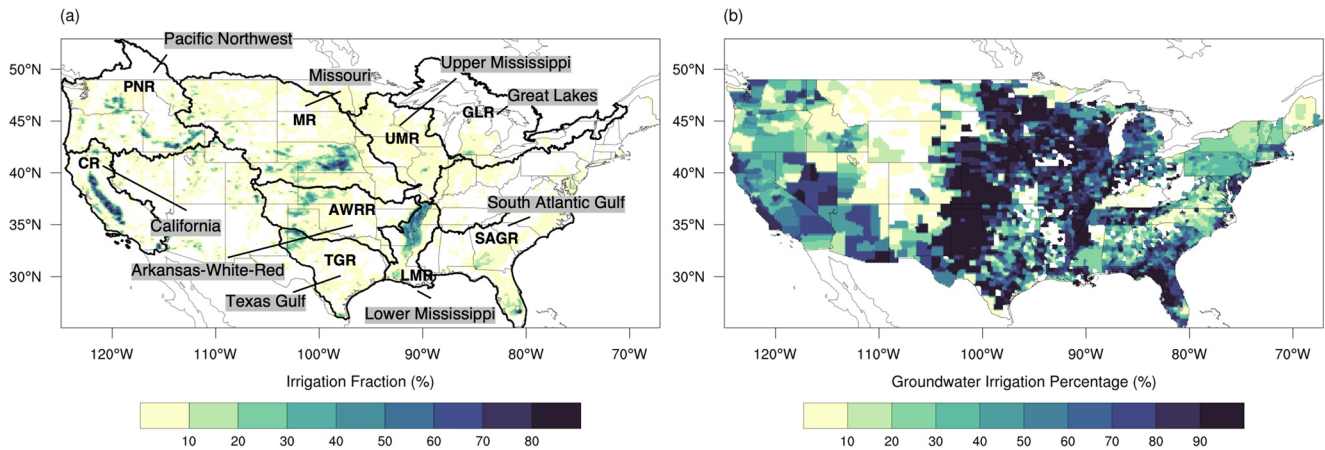


Figure 1. Distribution of irrigated area and groundwater irrigation. Panel (a) shows the long-term averaged irrigation fraction from the MODIS Irrigated Agriculture Data set for the United States upscaled from a spatial resolution of 250 m to the model resolution of 0.125° along with the water resource regions and panel (b) shows percent of irrigation from groundwater derived from the USGS water use report data given at county level.

Upper Mississippi Region (UMR), and South Atlantic-Gulf region (SAGR) are supported by a mix of both surface and groundwater irrigation.

We first compare the simulated and USGS reported irrigation water use from groundwater and surface water for the top 10 irrigated states for the years 2005, 2010, and 2015 (Figure 2). Compared to USGS reports, DA_{irr} in general better captures the magnitude and relative distribution of irrigation amount across different states than OL_{irr} . With the default prognostic phenology scheme, OL_{irr} estimates much larger irrigation water use, especially for Texas. A plausible explanation for this overestimation is that Noah-MP has large errors in the seasonal evolution of vegetation phenology due to the simplified parameterization of growth characteristics and the stomatal response to stresses, reported in previous studies (Liu et al., 2016; Niu et al., 2020). The limitations in capturing the magnitude and phase of vegetation growth in OL_{irr} influence vegetation and root zone soil moisture estimates in the model, which then impact the calculation of the amount of irrigation to be applied. As a result, the deficiencies in the GVF and root zone estimates in OL_{irr} lead to degradations in the irrigation water use estimates. By assimilating LAI, DA_{irr} reduces the irrigation water use estimates for nine out of 10 states while increasing the estimation for Nebraska. The relative irrigation usage across these 10 states in DA_{irr} is then much closer to the reported estimates. Note that the simulated quantities are still lower than the USGS estimates because the irrigation approach adopted by the model does not account for off-field losses and other inefficiencies. Besides, since the USGS report has its own uncertainties relating to data collection and quality control methods, its limited temporal coverage under such uncertainties does not allow for an evaluation of the irrigation use in terms of its interannual variability.

As of 2015, the USGS report began to provide consumptive irrigation water use estimates, which serve as a more comparable reference to the simulated water use. We regress the simulated state-level irrigation water amount from OL_{irr} and DA_{irr} onto the USGS consumptive water use and we find that the regressed model with DA_{irr} can explain 79% of the variance as compared to OL_{irr} with only 69%. The OL_{irr} simulated water use regressed on the reported consumptive use has a slope of 1.32 ± 0.27 at 95% confidence interval, indicating that on average the model may overestimate by about 5%–59% relative to consumptive use reports, with a significance test indicating that the slope is different from 1. DA_{irr} on the other hand, provides a closer statistical match to the USGS reports with a slope of 0.97 ± 0.15 , closer to the value of 1. The slope estimation of one indicates that the scale of water use among states between the USGS reports and the simulation is comparable. We also estimate the Pearson's correlation coefficient between the simulated and USGS water use to examine the spatial match and we find that DA_{irr} leads to correlation increasing from 0.83 for OL_{irr} to 0.89, but this difference is not statistically significant. These results underscore large uncertainties in irrigation water use estimation when relying on the prognostic phenology scheme within Noah-MP and highlight the value of assimilating LAI to constrain the irrigation simulation by correcting for the vegetation conditions. Further, the use of remote sensing LAI constraints also provides comparable and even better performance against the approach of prescribing vegetation conditions using monthly time-varying GVF data sets.

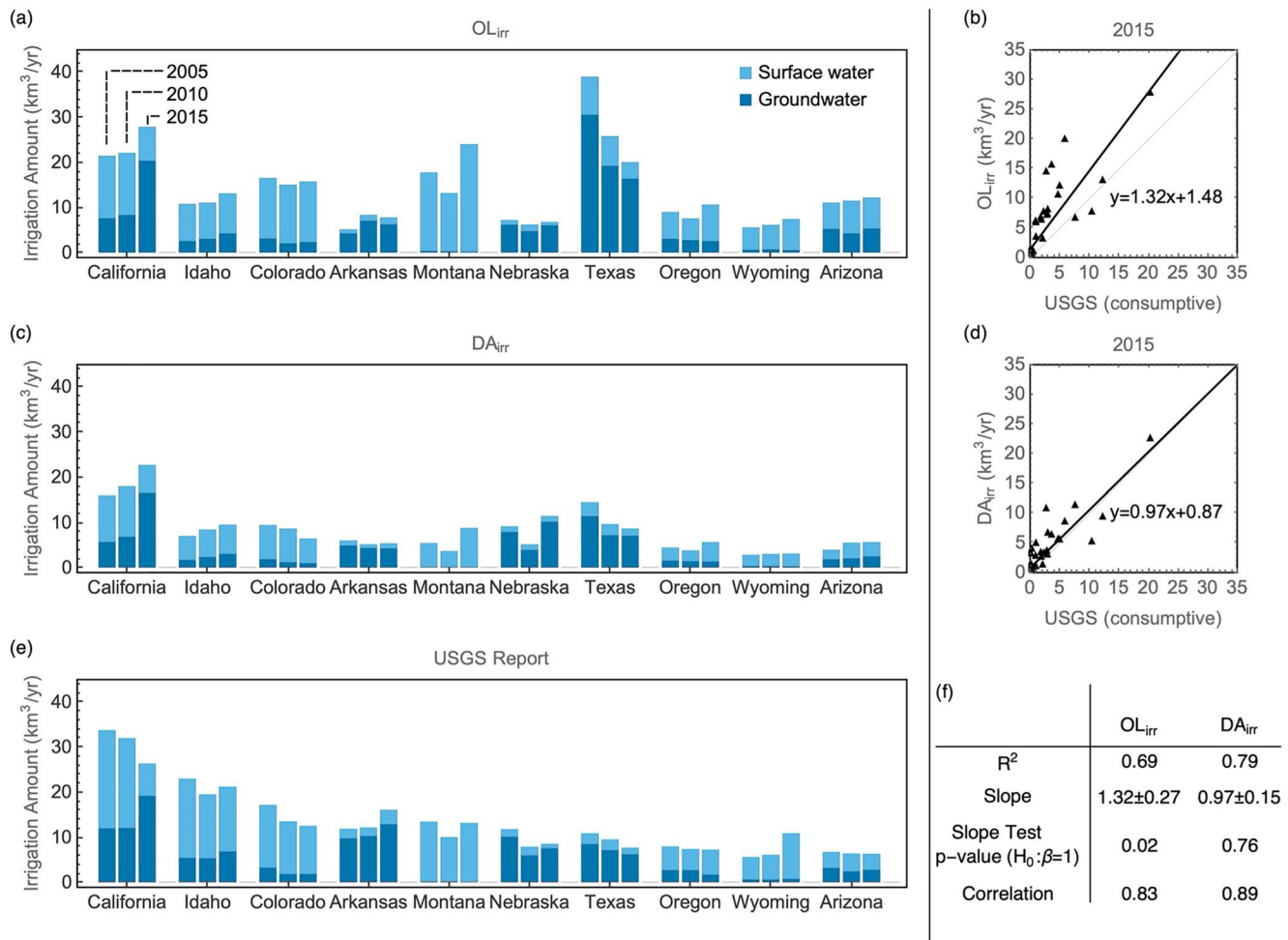


Figure 2. Comparison between simulated and USGS-reported irrigation water use. Panels (a, c, and e) show the simulated and USGS-reported groundwater and surface water irrigation amount for the top 10 irrigated states, selected and ranked based on USGS total irrigation amount for 2005, 2010, and 2015; panel (b and d) show the scatter plot of simulated total against USGS consumptive irrigation amount for 2015, along with (f) listing the statistics from linear regression and correlation analysis.

3.2. Surface Soil Moisture

Surface soil moisture is directly affected by both vegetation water uptake and irrigation, the signal of which can be retrieved from satellite measurements. To investigate the isolated and combined impact of irrigation and LAI assimilation on surface soil moisture distributions for actively irrigated areas, we use the Kullback-Leibler divergence (KLD; Kullback & Leibler, 1951) metric, a statistical measure of the difference in two probability distributions. Here we use it to compare the probability distribution differences between THySM surface soil moisture retrievals and the simulations for period 2015–2019. Note that the climatological seasonal cycle has been removed from the daily surface soil moisture before estimating KLD. Figure 3a shows the KLD of OL relative to THySM, with smaller values indicating closer agreement in the soil moisture distributions of OL and THySM, whereas larger KLD values indicate locations where they differ. Panels 3b–3d show the differences in KLD from various integrations relative to that from OL. In these panels, negative values of KLD differences indicate areas where there is a closer match with THySM. Conversely, positive values of KLD differences indicate locations where the respective integration worsens the level of agreement with THySM (relative to that in OL). Despite its tendency to overestimate irrigation amount, OL_{irr} leads to a better match with THySM over most of the irrigated areas compared to OL except for the western part of High Plains and Florida, which may stem from the mismatch in irrigation timing between the simulation and signals detected by THySM. This suggests that simulating irrigation can substantially affect the surface soil moisture anomaly distribution, and part of these irrigation signals are consistent with the estimates from the THySM product. For DA, improvements are only seen in Missouri

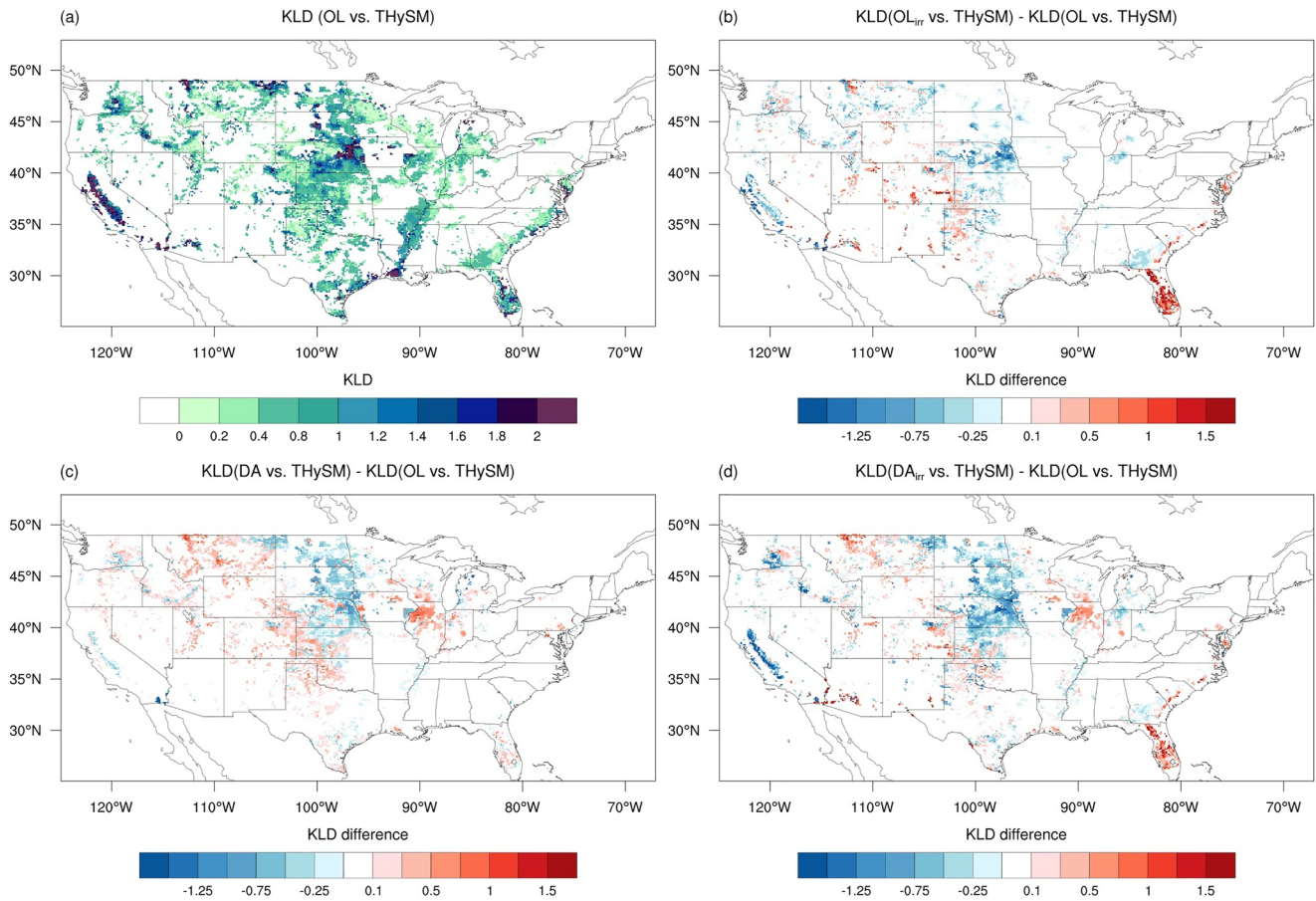


Figure 3. Impact of irrigation and leaf area index assimilation on surface soil moisture. Panel (a) shows the Kullback-Leibler divergence (KLD) estimates for OL against the THySM soil moisture retrievals, and panel (b–d) show the difference of KLD between OL against THySM and the other three simulations against Thermal Hydraulic disaggregation of Soil Moisture (THySM), respectively. Cool colors indicate a closer match with THySM while warm colors indicate larger differences with THySM.

and California, likely due to a correction of vegetation phase, while it leads to degradation in other regions. By constraining irrigation via assimilating LAI, DA_{irr} leads to overall largest improvements over California, followed by Pacific Northwest and Missouri. Note that irrigation signals with smaller amount of water applied and at scales smaller than ~ 9 km resolution are likely to be undetectable by SMAP (Lawston et al., 2017), limiting the utility of THySM product in representing the influence of irrigation on soil moisture conditions in such areas. Such representativeness limitations likely contribute to the mixed results found over the southern High Plains including Arkansas-White-Red and TGR. Additionally, THySM may observe faster soil moisture dry downs due to tile drainage in places like Midwest. Artificial drainage is not currently represented in the model, so assimilating LAI may drive simulated surface soil moisture further from THySM via modification of the vegetation and soil moisture interaction.

3.3. Evapotranspiration (ET)

To investigate the impact of LAI assimilation and irrigation on ET, we compare the four simulations for actively irrigated grid cells in each water resource region. The actively irrigated areas are divided into three classes: (a) lightly irrigated areas, where the irrigation fraction is lower than 20%; (b) moderately irrigated areas, where the irrigation fraction is within 20%–50%; and (c) heavily irrigated areas, where the irrigation fraction is greater than 50% (Figure 1a). Figures 4a–4f shows the correlation (R) and bias (BIAS) for simulated ET compared against ALEXI ET data set. DA_{irr} increases the correlation especially for the heavily irrigated category, with the median of the R improvement ranging from 0.07 to 1.1. The greatest improvement again is found for California with irrigation fraction greater than 50%, where the median of R increases from -0.21 in OL to 0.9 in DA_{irr} . However, the

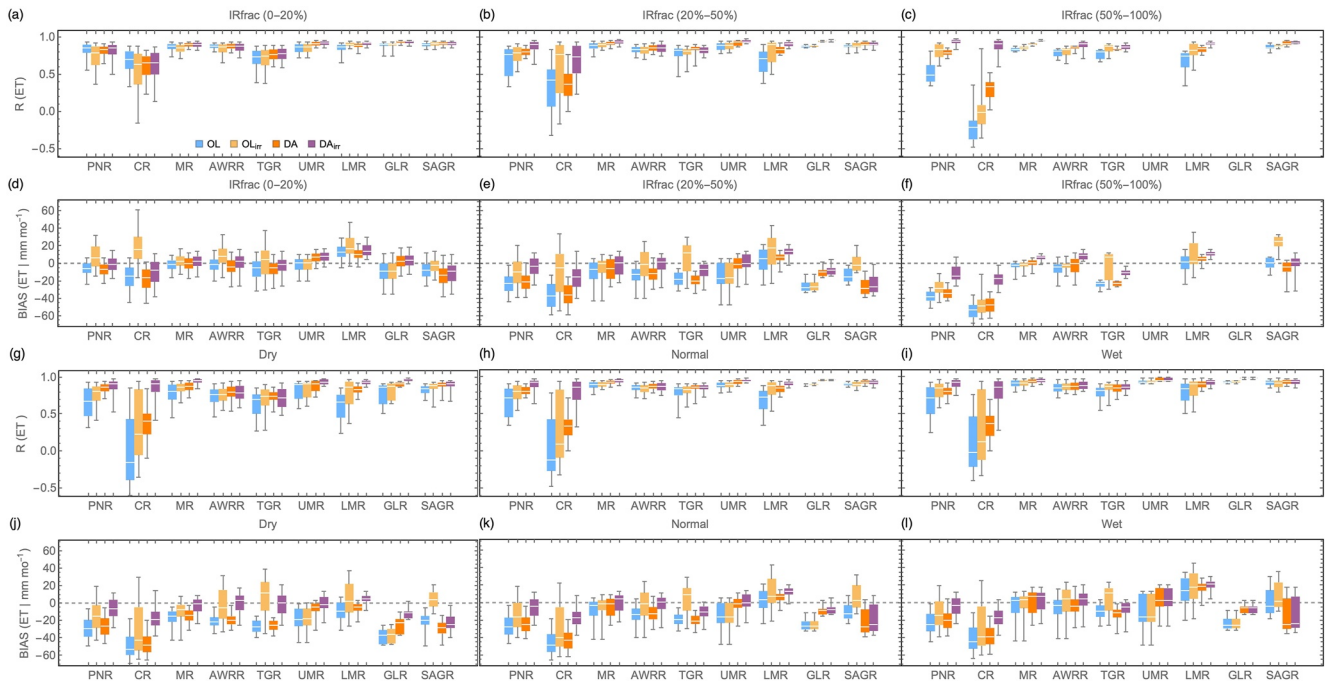


Figure 4. Impact of irrigation and leaf area index assimilation on evapotranspiration. Panel (a–f) show boxplots of the correlation (R) and BIAS averaged over actively irrigated areas for nine water resource regions with low (left column), moderate (middle column), and high (right column) irrigation fraction intensities for the OL, OL_{irr}, DA, and DA_{irr} simulations. Panel (g–i) show boxplots of R and BIAS averaged over actively irrigated areas for nine water resource regions stratified by dry (left column), normal (middle column), and wet (right column) conditions determined by precipitation anomalies.

impacts of either OL_{irr} or DA, in this case, are limited. In general, OL tends to underestimate ET for most of the regions, while DA_{irr} reduces the BIAS, in particular for Pacific Northwest, California and TGR, by an average of 14–35 mm/mo. Note that the improvement from DA_{irr} is not purely due to a fortuitous correction of a model bias. Over the Lower Mississippi and South Atlantic–Gulf, OL_{irr} overestimates ET which is also improved by DA_{irr} by reducing the amplitude of LAI. On one hand, LAI affects the irrigation demand via root depth parameterization, thus impacting ET by altering the water supply. On the other hand, LAI determines GVF, which affects ET by altering the evaporation and transpiration partitioning.

The contribution of DA_{irr} in improving the ET estimation stratified by dry, wet, and normal conditions are examined in Figures 4g–4i. The dry, wet, and normal years are defined as the z-score of the annual total precipitation less than -1 , greater than 1 , and in between, respectively within the period 2003–2019. Overall, the impact of DA_{irr} is generally insensitive to these moisture-based stratifications. Nevertheless, some instances of the influence of climate conditions are also observed in these results. For example, DA_{irr} exhibits greater improvements in ET correlation in dry years, with median correlation increased by 0.22 compared to OL across the nine regions, while the median increase is only by 0.1 for normal and by 0.08 for wet conditions. The greatest improvements are particularly found for Missouri and Great Lakes. The general contribution toward reducing biases, however, is similar regardless of the three moisture regimes. Overall, the combination of LAI assimilation and irrigation provides beneficial impacts in improving the magnitude and seasonal dynamics of ET, especially for intensively irrigated areas.

3.4. Gross Primary Production (GPP)

The same metrics as in the ET evaluation are used to examine the simulated impact on gross primary product compared against the FLUXSAT GPP product (Figures 5a–5f). For most of the irrigated regions, the improvements in GPP are mainly attributed to LAI assimilation rather than irrigation. OL_{irr} provides marginal impacts on GPP in most cases while assimilating LAI leads to substantial improvements in terms of R and BIAS for all regions across different irrigation intensity classes. The largest improvements take place over Missouri, Texas Gulf, Upper, and LMR, with median R increasing by 0.27, 0.29, 0.34, and 0.37 accounting for all irrigated areas,

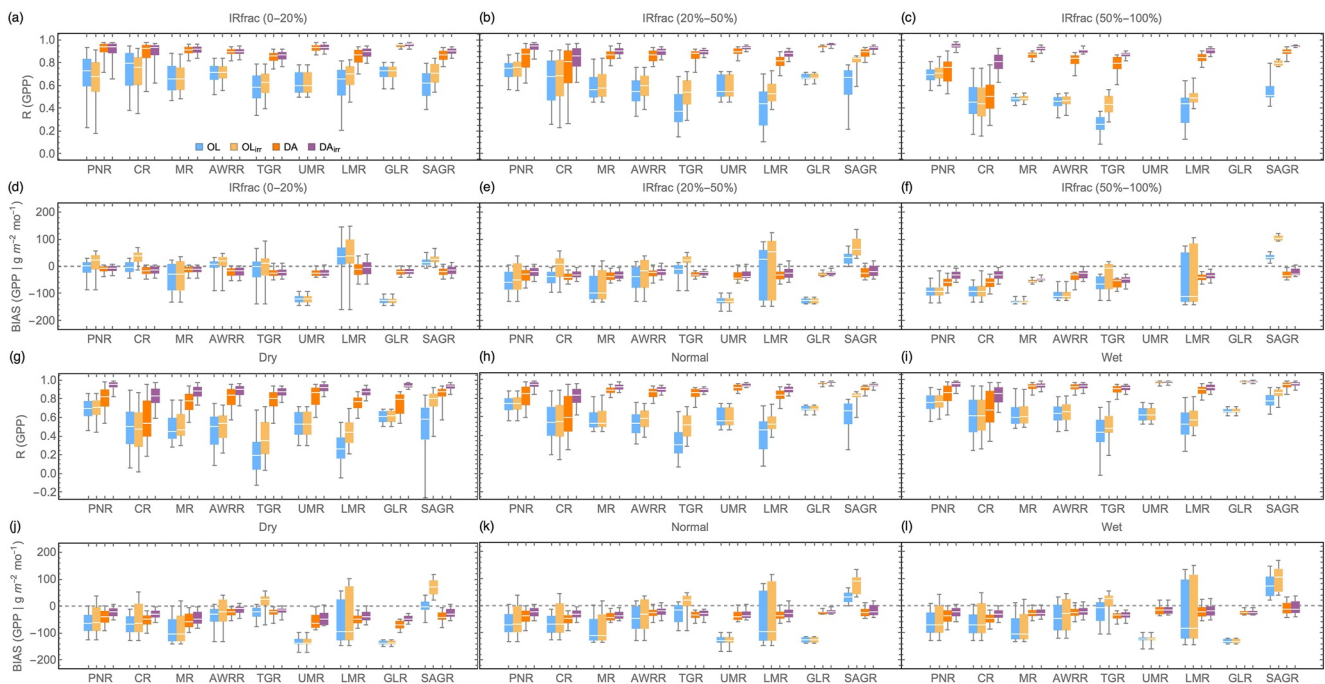


Figure 5. Same as Figure 4, but for gross primary production.

respectively. These improvements are mainly achieved by correcting for the seasonal phase of LAI, leading to an earlier onset of growing seasons. For these regions, DA_{irr} has additional, but marginal improvements on top of assimilating LAI. However, it is interesting to note that for heavily irrigated Pacific Northwest and California, DA alone does not dramatically improve the simulation of the seasonal variation of GPP (Figure 5c). The simultaneous use of irrigation and DA (DA_{irr}), on the other hand, provides more significant improvements. This indicates that an irrigation routine, in combination with assimilating observed vegetation conditions, plays a vital role in improving the simulation of carbon fluxes. The fact that DA_{irr} outperforms OL_{irr} also indicates that, besides a direct impact on carbon flux via assimilating LAI, the assimilation serves a critical role in supporting a better representation of irrigation processes. Interestingly, when categorized by precipitation anomalies, DA_{irr} shows greater capability in reducing GPP bias in normal to wet years for Upper Mississippi and Great Lakes, with the median of the BIAS further reduced by 7%–25% for the two regions as compared to that in dry years (Figures 5j–5l). However, the contribution on the correlation is not sensitive to climate conditions (Figures 5g–5i).

4. Discussion and Conclusions

This study investigates the role of assimilating remotely sensed LAI into the Noah-MP land surface model in improving the estimation of irrigation water use and associated fluxes. Results suggest that assimilating LAI to inform irrigation scheduling and demand estimation leads to significant improvements in the spatial distribution and magnitude of irrigation water use estimates when regressed to the USGS reported consumptive water use. It improves the simulated temporal evolution of surface soil moisture, ET, and GPP, with the median correlation increasing between 0.1–1.1 and 0.3–0.6 for ET and GPP, respectively, for heavily irrigated areas. The combination of irrigation and LAI data assimilation also effectively reduces the BIAS by 14–35 mm mo^{-1} for ET and 10–82 $\text{g m}^{-2} \text{mo}^{-1}$ for GPP for heavily irrigated areas. Large improvements found in California and PNR imply that capturing the vegetation variability and representing irrigation is crucial to better capture the seasonal dynamics of soil moisture and carbon fluxes for Mediterranean-like climate zones, as better vegetation seasonality supports better identification of irrigation time window, at which the applied water source is a major contributor to vegetation transpiration and soil evaporation. This, in turn, improves the vegetation phenology by providing more reliable water stress conditions. Besides, the large improvements in simulating water-energy-carbon fluxes in CR can be valuable in aiding water management and planning considering its role as the largest irrigation water consumer across CONUS facing challenges such as frequent drought, water shortages, and sustainable

groundwater use. Integrating models and satellite observations for irrigation estimation also reduces uncertainties as compared to single source satellite-based irrigation estimation as the satellite estimation contains noises and errors in its raw data, along with its uncertainties in the underlying retrieval algorithms (Foster et al., 2020). Our results demonstrate the effectiveness of utilizing satellite observed vegetation conditions to overcome the model errors in simulating vegetation phenology and the potential to compensate for simplified irrigation parameterization to improve the spatiotemporal variation of irrigation in response to climate and agricultural land use change. Such information is essential for more informed management of global freshwater withdrawals and benefit the understanding of anticipate climate change impacts on future water availability. It could also support impact studies for human-water interactions such as irrigation in response to extremes. This approach can be incorporated into other land surface models and applied to irrigated regions over the globe. The strategy of assimilating LAI to constrain irrigation simulation is especially beneficial over regions where ground-based irrigation data and related measurements are not available for irrigation calibration. However, the effectiveness of such strategy would heavily rely on the capability of the remotely sensed measurements in detecting irrigation signals at the targeted spatial scale.

While the approach presented here can reasonably capture the pattern of irrigation estimation and its impact on fluxes for CONUS, reliable estimation of its sub-monthly variation remains challenging as the timing of irrigation in our scheme, which is determined by vegetation threshold parameter, coincides more with particularly vulnerable growth stages and irrigation is absent in early stages of the crop season before LAI reaches the threshold. Moreover, large uncertainties still exist for irrigation estimation globally due to the utilization of different irrigation area data sets, weather drivers, crop representations, and irrigation approaches (Scanlon et al., 2018; Wisser et al., 2008; Wada et al., 2017). Continuing improvements to reduce uncertainties for these aspects should remain a priority as this may further enhance the benefit of LAI assimilation-informed irrigation. Finally, our study identifies better model performance in western and central CONUS, while capturing the seasonal and inter-annual variations in energy and carbon fluxes over irrigated regions in the eastern U.S. remains a challenge. This is likely due to the limitation of the spatial resolution from both the model input and remote-sensing constraints in capturing irrigation detail in eastern U.S. irrigated fields, which have smaller irrigation extent, lower irrigated density, and supplementary irrigation signal compared to rainfall variability. This might be addressed through multivariate joint data assimilation to better constrain irrigation estimates. For instance, approaches to introduce soil moisture related constraints within irrigation formulations (e.g., Felfelani et al., 2018) indicate that the joint use of moisture and vegetation constraints also may be a fruitful future direction. Overall, our study demonstrates the strong influence that vegetation condition has in parameterizing irrigation and the effectiveness of assimilating LAI to an advanced land surface model in improving irrigation formulation and the associated water, energy, and carbon cycles in response to irrigation. Capturing these features is important for water resource assessment and for simulating human influence on land-atmosphere interactions in coupled land to weather and climate models.

Data Availability Statement

The modeling platform LIS along with Noah-MP land surface model used for this research is an open-source software available at <https://github.com/NASA-LIS/LISF>. Different datasets used for model evaluation are available from the following websites: MCD15A2H LAI: <https://lpdaac.usgs.gov/products/mcd15a2hv006/>; USGS Water Use Report: <https://water.usgs.gov/watuse/data/>; THySM available through USDA NASS: <https://nassgeo.csiss.gmu.edu/CropCASMA/>; FLUXSAT: https://avdc.gsfc.nasa.gov/pub/tmp/FluxSat_GPP/; ALEXI ET and the model output relevant to this work are available through the Johns Hopkins Data Archive (DOI: <https://doi.org/10.7281/T1/RECXQW>).

References

- Albergel, C., Munier, S., Leroux, D. J., Dewaele, H., Fairbairn, D., Barbu, A. L., et al. (2017). Sequential assimilation of satellite-derived vegetation and soil moisture products using SURFEX_v8. 0: LDAS-Monde assessment over the Euro-Mediterranean area. *Geoscientific Model Development*, 10(10), 3889–3912. <https://doi.org/10.5194/gmd-10-3889-2017>
- Anderson, M. C., Norman, J. M., Mecikalski, J. R., Otkin, J. A., & Kustas, W. P. (2007). A climatological study of evapotranspiration and moisture stress across the continental United States based on thermal remote sensing: 1. Model formulation. *Journal of Geophysical Research*, 112(D10). <https://doi.org/10.1029/2006jd007506>
- Asoka, A., Gleeson, T., Wada, Y., & Mishra, V. (2017). Relative contribution of monsoon precipitation and pumping to changes in groundwater storage in India. *Nature Geoscience*, 10(2), 109–117. <https://doi.org/10.1038/ngeo2869>

Acknowledgments

This work was supported by the NASA sponsored Earth Information System (EIS) pilot project. Computational resources were provided by the NASA's Center for Climate Simulation (NCCS).

- Ball, J. T., Woodrow, I. E., & Berry, J. A. (1987). A model predicting stomatal conductance and its contribution to the control of photosynthesis under different environmental conditions. In *Progress in photosynthesis research* (pp. 221–224). Springer.
- Barbu, A. L., Calvet, J. C., Mahfouf, J.-F., & Lafont, S. (2014). Integrating ASCAT surface soil moisture and GEOV1 leaf area index into the SURFEX modelling platform: A land data assimilation application over France. *Hydrology and Earth System Sciences Discussions*, *18*(1), 173–192. <https://doi.org/10.5194/hess-18-173-2014>
- Bonan, G. B. (1996). *Land surface model (LSM version 1.0) for ecological, hydrological, and atmospheric studies: Technical description and users guide*. National Center for Atmospheric Research. Climate and Global Dynamics Division. *Technical note* (No. PB-97-131494/XAB; NCAR/TN-417-STR).
- Brown, J. F., & Pervez, M. S. (2014). Merging remote sensing data and national agricultural statistics to model change in irrigated agriculture. *Agricultural Systems*, *127*, 28–40. <https://doi.org/10.1016/j.agsy.2014.01.004>
- Chan, S. K., Bindlish, R., O'Neill, P., Jackson, T., Njoku, E., Dunbar, S., et al. (2018). Development and assessment of the SMAP enhanced passive soil moisture product. *Remote Sensing of Environment*, *204*, 931–941. <https://doi.org/10.1016/j.rse.2017.08.025>
- Chen, Z., Yang, Z., Zhao, H., Sun, Z., Di, L., Bindlish, R., et al. (2022). Crop-CASMA: A web geoprocessing and map service based architecture and implementation for serving soil moisture and crop vegetation condition data over U.S. Cropland. *International Journal of Applied Earth Observation and Geoinformation*, *112*(427), 102902. <https://doi.org/10.1016/j.jag.2022.102902>
- Collatz, G. J., Ball, J. T., Grivet, C., & Berry, J. A. (1991). Physiological and environmental regulation of stomatal conductance, photosynthesis and transpiration: A model that includes a laminar boundary layer. *Agricultural and Forest Meteorology*, *54*(2–4), 107–136. [https://doi.org/10.1016/0168-1923\(91\)90002-8](https://doi.org/10.1016/0168-1923(91)90002-8)
- DeAngelis, A., Dominguez, F., Fan, Y., Robock, A., Kustu, M. D., & Robinson, D. (2010). Evidence of enhanced precipitation due to irrigation over the Great Plains of the United States. *Journal of Geophysical Research*, *115*(D15). <https://doi.org/10.1029/2010jd013892>
- Deines, J. M., Kendall, A. D., & Hyndman, D. W. (2017). Annual irrigation dynamics in the U.S. Northern high Plains derived from landsat satellite data. *Geophysical Research Letters*, *44*(18), 9350–9360. <https://doi.org/10.1002/2017GL074071>
- Demarty, J., Chevallier, F., Friend, A. D., Viovy, N., Piao, S., & Ciais, P. (2007). Assimilation of global MODIS leaf area index retrievals within a terrestrial biosphere model. *Geophysical Research Letters*, *34*(15). <https://doi.org/10.1029/2007gl030014>
- Dickinson, R. E., Shaikh, M., Bryant, R., & Graumlich, L. (1998). Interactive canopies for a climate model. *Journal of Climate*, *11*(11), 2823–2836. [https://doi.org/10.1175/1520-0442\(1998\)011<2823:icfacm>2.0.co;2](https://doi.org/10.1175/1520-0442(1998)011<2823:icfacm>2.0.co;2)
- Döll, P., Hoffmann-Dobrev, H., Portmann, F. T., Siebert, S., Eicker, A., Rodell, M., et al. (2012). Impact of water withdrawals from groundwater and surface water on continental water storage variations. *Journal of Geodynamics*, *59*, 143–156. <https://doi.org/10.1016/j.jog.2011.05.001>
- Farr, T. G., Rosen, P. A., Caro, E., Crippen, R., Duren, R., Hensley, S., et al. (2007). The shuttle radar topography mission. *Reviews of Geophysics*, *45*(2), RG2004. <https://doi.org/10.1029/2005rg000183>
- Felfelani, F., Pokhrel, Y., Guan, K., & Lawrence, D. M. (2018). Utilizing SMAP soil moisture data to constrain irrigation in the Community Land Model. *Geophysical Research Letters*, *45*(23), 12892–12902. <https://doi.org/10.1029/2018gl080870>
- Flörke, M., Lapola, D. M., Schaldach, R., Voß, F., & Teichert, E. (2010). Modelling historical and current irrigation water demand on the continental scale: Europe. *Advances in Geosciences*, *27*, 79–85. <https://doi.org/10.5194/adgeo-27-79-2010>
- Foster, T., Mieno, T., & Brozović, N. (2020). Satellite-based monitoring of irrigation water use: Assessing measurement errors and their implications for agricultural water management policy. *Water Resources Research*, *56*(11), e2020WR028378. <https://doi.org/10.1029/2020wr028378>
- Frenken, K., & Gillet, V. (2012). *Irrigation water requirement and water withdrawal by country*. FAO.
- Friedl, M. A., Sulla-Menashe, D., Tan, B., Schneider, A., Ramankutty, N., Sibley, A., & Huang, X. (2010). MODIS Collection 5 global land cover: Algorithm refinements and characterization of new datasets. *Remote Sensing of Environment*, *114*(1), 168–182. <https://doi.org/10.1016/j.rse.2009.08.016>
- Hengl, T., Mendes de Jesus, J., Heuvelink, G. B., Ruiperez Gonzalez, M., Kilibarda, M., Blagotić, A., et al. (2017). SoilGrids250m: Global gridded soil information based on machine learning. *PLoS One*, *12*(2), e0169748. <https://doi.org/10.1371/journal.pone.0169748>
- Ines, A. V. M., Das, N. N., Hansen, J. W., & Njoku, E. G. (2013). Assimilation of remotely sensed soil moisture and vegetation with a crop simulation model for maize yield prediction. *Remote Sensing of Environment*, *138*, 149–164. <https://doi.org/10.1016/j.rse.2013.07.018>
- Joiner, J., Yoshida, Y., Zhang, Y., Duveiller, G., Jung, M., Lyapustin, A., et al. (2018). Estimation of terrestrial global gross primary production (GPP) with satellite data-driven models and eddy covariance flux data. *Remote Sensing*, *10*(9), 1346–1438. <https://doi.org/10.3390/rs10091346>
- Kueppers, L. M., Snyder, M. A., & Sloan, L. C. (2007). Irrigation cooling effect: Regional climate forcing by land-use change. *Geophysical Research Letters*, *34*(3), L03703. <https://doi.org/10.1029/2006gl028679>
- Kullback, S., & Leibler, R. A. (1951). On information and sufficiency. *The Annals of Mathematical Statistics*, *22*(1), 79–86. <https://doi.org/10.1214/aoms/1177729694>
- Kumar, S. V., Mocko, D. M., Wang, S., Peters-Lidard, C. D., & Borak, J. (2019). Assimilation of remotely sensed leaf area index into the Noah-MP land surface model: Impacts on water and carbon fluxes and states over the continental United States. *Journal of Hydrometeorology*, *20*(7), 1359–1377. <https://doi.org/10.1175/JHM-D-18-0237.1>
- Kumar, S. V., Holmes, T. R., Bindlish, R., de Jeu, R., & Peters-Lidard, C. (2020). Assimilation of vegetation optical depth retrievals from passive microwave radiometry. *Hydrology and Earth System Sciences Discussions*, *24*(7), 3431–3450. <https://doi.org/10.5194/hess-24-3431-2020>
- Kumar, S. V., Peters-Lidard, C. D., Tian, Y., Houser, P. R., Geiger, J., Olden, S., et al. (2006). Land information system: An interoperable framework for high resolution land surface modeling. *Environmental Modelling & Software*, *21*(10), 1402–1415. <https://doi.org/10.1016/j.envsoft.2005.07.004>
- Kustu, M. D., Fan, Y., & Rodell, M. (2011). Possible link between irrigation in the US High Plains and increased summer streamflow in the Midwest. *Water Resources Research*, *47*(3). <https://doi.org/10.1029/2010wr010046>
- Lawston, P. M., Santanello, J. A., Jr., Hanson, B., & Arsensault, K. (2020). Impacts of irrigation on summertime temperatures in the Pacific Northwest. *Earth Interactions*, *24*(1), 1–26. <https://doi.org/10.1175/EI-D-19-0015.1>
- Lawston, P. M., Santanello, J. A., Jr., & Kumar, S. V. (2017). Irrigation signals detected from SMAP soil moisture retrievals. *Geophysical Research Letters*, *44*(23), 11860–11867. <https://doi.org/10.1002/2017gl075733>
- Lawston, P. M., Santanello, J. A., Jr., Zaitchik, B. F., & Rodell, M. (2015). Impact of irrigation methods on land surface model spinup and initialization of WRF forecasts. *Journal of Hydrometeorology*, *16*(3), 1135–1154. <https://doi.org/10.1175/jhm-d-14-0203.1>
- Leng, G., Huang, M., Tang, Q., Gao, H., & Leung, L. R. (2014). Modeling the effects of groundwater-fed irrigation on terrestrial hydrology over the conterminous United States. *Journal of Hydrometeorology*, *15*(3), 957–972. <https://doi.org/10.1175/jhm-d-13-049.1>
- Leng, G., Huang, M., Tang, Q., & Leung, L. R. (2015). A modeling study of irrigation effects on global surface water and groundwater resources under a changing climate. *Journal of Advances in Modeling Earth Systems*, *7*(3), 1285–1304. <https://doi.org/10.1002/2015ms000437>

- Li, L., Yang, Z. L., Matheny, A. M., Zheng, H., Swenson, S. C., Lawrence, D. M., et al. (2021). Representation of plant hydraulics in the Noah-MP land surface model: Model development and multi-scale evaluation. *Journal of Advances in Modeling Earth Systems*, *13*(4), 1–57. <https://doi.org/10.1029/2020MS002214>
- Liu, P.-W., Bindlish, R., O'Neill, P. E., Fang, B., Lakshmi, V., Yang, Z., et al. (2022). Thermal hydraulic disaggregation of SMAP soil moisture over the continental United States. *Ieee Journal of Selected Topics in Applied Earth Observations and Remote Sensing*, *15*, 4072–4092. <https://doi.org/10.1109/JSTARS.2022.3165644>
- Liu, X., Chen, F., Barlage, M., Zhou, G., & Niyogi, D. (2016). Noah-MP-Crop: Introducing dynamic crop growth in the Noah-MP land surface model. *Journal of Geophysical Research: Atmospheres*, *121*(23), 13953–13972. <https://doi.org/10.1002/2016JD025597>
- Lobell, D. B., Bonfils, C. J., Kueppers, L. M., & Snyder, M. A. (2008). Irrigation cooling effect on temperature and heat index extremes. *Geophysical Research Letters*, *35*(9), L09705. <https://doi.org/10.1029/2008gl034145>
- Ma, N., Niu, G. Y., Xia, Y., Cai, X., Zhang, Y., Ma, Y., & Fang, Y. (2017). A systematic evaluation of Noah-MP in simulating land-atmosphere energy, water, and carbon exchanges over the continental United States. *Journal of Geophysical Research: Atmospheres*, *122*(22), 12245–12268. <https://doi.org/10.1002/2017jd027597>
- Mocko, D. M., Kumar, S. V., Peters-Lidard, C. D., & Wang, S. (2021). Assimilation of vegetation conditions improves the representation of drought over agricultural areas. *Journal of Hydrometeorology*, *22*(5), 1085–1098. <https://doi.org/10.1175/JHM-D-20-0065.1>
- Myneni, R., Knyazikhin, Y., & Park, T. (2015). MCD15A2H MODIS/Terra+Aqua leaf area index/FPAR 8-day L4 global 500m SIN grid V006 [Dataset]. NASA EOSDIS Land Processes DAAC. <https://doi.org/10.5067/MODIS/MCD15A2H.006>
- Nie, W., Zaitchik, B. F., Rodell, M., Kumar, S. V., Anderson, M. C., & Hain, C. (2018). Groundwater withdrawals under drought: Reconciling GRACE and land surface models in the United States High Plains Aquifer. *Water Resources Research*, *54*(8), 5282–5299. <https://doi.org/10.1029/2017wr022178>
- Nie, W., Zaitchik, B. F., Rodell, M., Kumar, S. V., Arsenault, K. R., & Badr, H. S. (2021). Irrigation water demand sensitivity to climate variability across the Contiguous United States. *Water Resources Research*, *57*(3), 2020WR027738. <https://doi.org/10.1029/2020wr027738>
- Niu, G. Y., Fang, Y. H., Chang, L. L., Jin, J., Yuan, H., & Zeng, X. (2020). Enhancing the Noah-MP ecosystem response to droughts with an explicit representation of plant water storage supplied by dynamic root water uptake. *Journal of Advances in Modeling Earth Systems*, *12*(11), 1–29. <https://doi.org/10.1029/2020MS002062>
- Niu, G. Y., Yang, Z. L., Mitchell, K. E., Chen, F., Ek, M. B., Barlage, M., et al. (2011). The community Noah land surface model with multiparameterization options (Noah-MP): 1. Model description and evaluation with local-scale measurements. *Journal of Geophysical Research*, *116*(D12), 1381–1419. <https://doi.org/10.1029/2010JD015139>
- Ozdogan, M., Rodell, M., Beaudoin, H. K., & Toll, D. L. (2010). Simulating the effects of irrigation over the United States in a land surface model based on satellite-derived agricultural data. *Journal of Hydrometeorology*, *11*(1), 171–184. <https://doi.org/10.1175/2009jhm1116.1>
- Pokhrel, Y. N., Koirala, S., Yeh, P. J.-F., Hanasaki, N., Longuevergne, L., Kanae, S., & Oki, T. (2015). Incorporation of groundwater pumping in a global land surface model with the representation of human impacts. *Water Resources Research*, *51*(1), 78–96. <https://doi.org/10.1002/2014wr015602>
- Reichle, R. H., Koster, R. D., Liu, P., Mahanama, S. P., Njoku, E. G., & Owe, M. (2007). Comparison and assimilation of global soil moisture retrievals from the advanced microwave scanning radiometer for the Earth observing system (AMSR-E) and the scanning multichannel microwave radiometer (SMMR). *Journal of Geophysical Research*, *112*(D9), D09108. <https://doi.org/10.1029/2006jd008033>
- Reichle, R. H., McLaughlin, D. B., & Entekhabi, D. (2002). Hydrologic data assimilation with the ensemble Kalman filter. *Monthly Weather Review*, *130*(1), 103–114. [https://doi.org/10.1175/1520-0493\(2002\)130<0103:hdawte>2.0.co;2](https://doi.org/10.1175/1520-0493(2002)130<0103:hdawte>2.0.co;2)
- Rodell, M., Famiglietti, J. S., Wiese, D. N., Reager, J. T., Beaudoin, H. K., Landerer, F. W., & Lo, M.-H. (2018). Emerging trends in global freshwater availability. *Nature*, *557*(7707), 651–659. <https://doi.org/10.1038/s41586-018-0123-1>
- Russo, T. A., & Lall, U. (2017). Depletion and response of deep groundwater to climate-induced pumping variability. *Nature Geoscience*, *10*(2), 105–108. <https://doi.org/10.1038/ngeo2883>
- Scanlon, B. R., Faunt, C. C., Longuevergne, L., Reedy, R. C., Alley, W. M., McGuire, V. L., & McMahon, P. B. (2012). Groundwater depletion and sustainability of irrigation in the US high Plains and Central Valley. *Proceedings of the National Academy of Sciences of the United States of America*, *109*(24), 9320–9325. <https://doi.org/10.1073/pnas.1200311109>
- Scanlon, B. R., Zhang, Z., Save, H., Sun, A. Y., Schmied, H. M., Van Beek, L. P., et al. (2018). Global models underestimate large decadal declining and rising water storage trends relative to GRACE satellite data. *Proceedings of the National Academy of Sciences of the United States of America*, *115*(6), E1080–E1089. <https://doi.org/10.1073/pnas.1704665115>
- Troy, T. J., Kipgen, C., & Pal, I. (2015). The impact of climate extremes and irrigation on US crop yields. *Environmental Research Letters*, *10*(5), 054013. <https://doi.org/10.1088/1748-9326/10/5/054013>
- Trugman, A. T., Medvigy, D., Mankin, J. S., & Anderegg, W. (2018). Soil moisture stress as a major driver of carbon cycle uncertainty. *Geophysical Research Letters*, *45*(13), 6495–6503. <https://doi.org/10.1029/2018gl078131>
- Wada, Y., Bierkens, M. F., De Roo, A., Dirmeyer, P. A., Famiglietti, J. S., Hanasaki, N., et al. (2017). Human-water interface in hydrological modelling: Current status and future directions. *Hydrology and Earth System Sciences*, *21*(8), 4169–4193. <https://doi.org/10.5194/hess-21-4169-2017>
- Wada, Y., Wisser, D., & Bierkens, M. F. P. (2014). Global modeling of withdrawal, allocation and consumptive use of surface water and groundwater resources. *Earth System Dynamics*, *5*(1), 15–40. <https://doi.org/10.5194/esd-5-15-2014>
- Wisser, D., Frolking, S., Douglas, E. M., Fekete, B. M., Vörösmarty, C. J., & Schumann, A. H. (2008). Global irrigation water demand: Variability and uncertainties arising from agricultural and climate data sets. *Geophysical Research Letters*, *35*(24), L24408. <https://doi.org/10.1029/2008gl035296>
- Wu, L., Feng, J., & Miao, W. (2018). Simulating the impacts of irrigation and dynamic vegetation over the North China Plain on regional climate. *Journal of Geophysical Research: Atmospheres*, *123*(15), 8017–8034. <https://doi.org/10.1029/2017jd027784>
- Xia, Y., Mitchell, K., Ek, M., Sheffield, J., Cosgrove, B., Wood, E., et al. (2012). Continental-scale water and energy flux analysis and validation for the North American land data assimilation system project phase 2 (NLDAS-2): 1. Intercomparison and application of model products. *Journal of Geophysical Research*, *117*(D3). <https://doi.org/10.1029/2011jd016048>
- Xie, Y., Wang, P., Bai, X., Khan, J., Zhang, S., Li, L., & Wang, L. (2017). Assimilation of the leaf area index and vegetation temperature condition index for winter wheat yield estimation using Landsat imagery and the CERES-Wheat model. *Agricultural and Forest Meteorology*, *246*, 194–206. <https://doi.org/10.1016/j.agrformet.2017.06.015>
- Yamazaki, D., Ikeshima, D., Tawatari, R., Yamaguchi, T., O'Loughlin, F., Neal, J. C., et al. (2017). A high-accuracy map of global terrain elevations. *Geophysical Research Letters*, *44*(11), 5844–5853. <https://doi.org/10.1002/2017gl072874>
- Yilmaz, M. T., Anderson, M. C., Zaitchik, B., Hain, C. R., Crow, W. T., Ozdogan, M., et al. (2014). Comparison of prognostic and diagnostic surface flux modeling approaches over the Nile River basin. *Water Resources Research*, *50*(1), 386–408. <https://doi.org/10.1002/2013wr014194>

- Zaveri, E., & Lobell, D. B. (2019). The role of irrigation in changing wheat yields and heat sensitivity in India. *Nature Communications*, *10*(1), 1–7. <https://doi.org/10.1038/s41467-019-12183-9>
- Zeng, Y., Xie, Z., & Zou, J. (2017). Hydrologic and climatic responses to global anthropogenic groundwater extraction. *Journal of Climate*, *30*(1), 71–90. <https://doi.org/10.1175/jcli-d-16-0209.1>
- Zhao, G., Webber, H., Hoffmann, H., Wolf, J., Siebert, S., & Ewert, F. (2015). The implication of irrigation in climate change impact assessment: A European-wide study. *Global Change Biology*, *21*(11), 4031–4048. <https://doi.org/10.1111/gcb.13008>